ATLAS NOTE

ATL-MUON-COM-2009-XXX

June 4, 2009

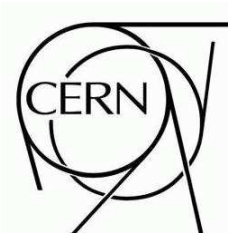

Standalone studies with muons

A. Belloni, K.M. Black, G. Brandenburg, J. Guimaraes da Costa, V.I. Martinez Outschoorn, S. Prasad

Abstract

We present some standalone ROOT-based studies that have been performed to understand and characterize the performance of the Moore segment-fitting procedure, and to understand details of calibration as they affect segment performance. We find that the extra effect imposed upon segment residuals by the procedure of in-situ t_0 calibration is at the sub-micron level, and that jitter and time-of-flight based effects upon hit times are removed, with the correct hit time extracted from the fit. We observe further the stability of the procedure under conditions of imperfect seed segments. We note that using a single t_0 per chamber in the conditions database imposes a 10-50 micron penalty upon the segment residuals depending upon topology. Finally, we reemphasize the vital importance of having up-to-date, temperature corrected RT functions by demonstrating the effect of temperature variation across the detector, and of having RT functions hours or a week out of sync with the data.

1 Motivation

Muons in ATLAS are detected using the Muon Spectrometer, which is embedded in a toroidal $2T$ field. In the bending / precision / η direction defined by this field, measurements of the muon are made by a series of **M**onitored **D**rift **T**ube (MDT) chambers. Each gas-filled tube provides a measurement, or hit, which gives the drift radius of any muon passing through it. Given a series of such hits, sophisticated muon reconstruction algorithms work backward to recover the muon, its momentum, charge and spatial information. Our work in particular is carried out in the context of the **M**uon **O**bject **O**riented **RE**construction (MOORE) algorithm. MOORE begins with the regions of interest provided by the trigger chambers, and uses Hough transform based methods to find *patterns* of hits in the bending and non-bending planes, which are then combined to form *roads*. Then, within a road, extreme hits are used to generate all possible tangent lines, which seed the candidate straight line *segments* that are fitted to the hits. Finally, the selected segments seed a full track reconstruction, which incoroprates a detailed description of the magnetic field, material description etc to form curved tracks. For this procedure to function, an important requirement is the calibration of the hits themselves.

First, one must correctly extract the *time* that the hits' electronic signal corresponds to. That is, given a trigger, we must know how far back in time we must go to collect the hit signal. Now, muons passing very close to the drift wire present a near-immediate signal to the chamber electronics, while muons at glancing tube incidence must propagate a signal through ionizing gas across a whole tube radius in order to make a signal at the drift wire. Hence, to extract the muon signal, me must know the difference in time between trigger passage and the time that a muon passing through a drift wire goes through the tube. This difference, known as t_0 (Fig. 1), includes a variety of factors, chief of which are the L1 trigger latency, and the lengths of the fibers and cables for both trigger and MDT chambers. In order to extract the signal therefore, the DAQ system must encode knowledge of these latencies and lengths, ideally on a per-tube basis. In practice, this includes a determination, at dedicated calibration centers, of t_0's from fits of TDC spectra seen in data.

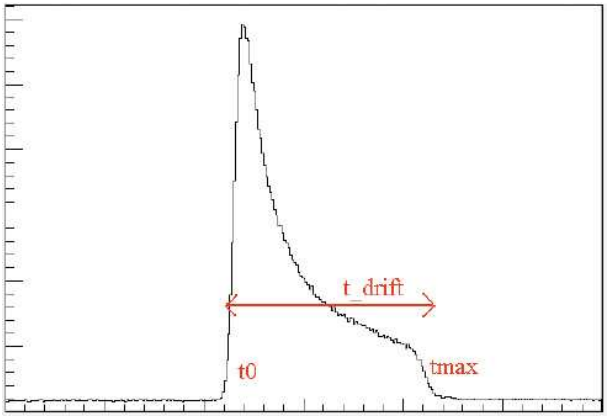

Figure 1: t_0 from TDC spectrum

Currently, there are additional issues to consider however. First, cosmic rays present an intrinsic 25 ns timing *jitter* because cosmics do not come in sync with the LHC clock. Further, the time of flight is not known because the muon may be coming from anywhere instead of being produced at the interaction point as one would typically see with beam data. Also, at the present stage of commissioning, marked by changes to the trigger setup that aren't necessarily incorporated into the database immediately, it isn't always practical to expect that the t_0 in the system corresponds to the true value. Further, the

limited statistics currently available in cosmic ray data mean that often only per-chamber t_0 information is available. To account for such issues, all except the last of which are all well characterized by a single segment-level shift to the t_0, we have implemented an Athena/MOORE based package that shifts hit times by an offset even as it fits for segment position and angle. This three parameter, so-called t_0-fitter is currently incorporated into the MOORE reconstruction package for cosmic rays. Its performance has been documented elsewhere [1]; for now we remark that the procedure leads to a factor of two in segment residuals observed with cosmic muons.

Next, we must have confidence that our extraction of the hit *radius* from the hit *time* does in fact provide the actual muon distance from the drift wire. In other words, the RT function we use must be well understood and descriptive of the tube physics. Again, the calibration centers are tasked with providing calibrated RT functions, that account for effects like temperature variation in the detector, and the gas composition is carefully monitored. The visual appearance of RT functions may be gleaned from Fig. 2; one important aspect of these functions is their non-linearity, especially at small radius / close to the drift-wire, where the high field makes the gas highly non-linear. Further, such calibrations must be up-to-date, ideally over the range of a few hours, so that they correspond to the conditions under which data were actually taken. For example, note that the time-radius map in Fig. 2 is noticeably different for two different time periods. This is especially so at high radius/time, where differing gas properties and temperature have had most impact upon the signal traveling to the wire. In our present commissioning work, however, it isn't necessarily the case that we have RT functions at the individual chamber level, and calibrations may in addition be out of date.

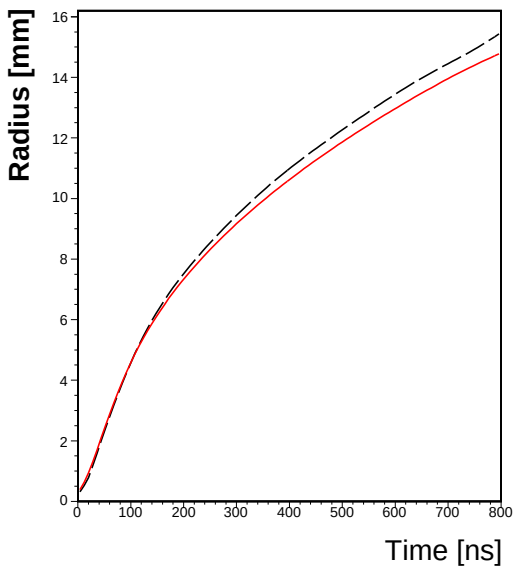

Figure 2: Drift circle radius versus drift time. The black/dashed curve is our default RT function, from mid-2008. The solid/red function is another, corresponding to detector conditions during the morning of 28th January 2009.

The present work is an effort to understand the effect of hit timing and radius calibration upon observed muon reconstruction performance, as we isolate various effects in a standalone reproduction of parts of the muon code. Such a reproduction also enables us to characterize the significant tails seen in residual distributions for cosmic muons acquired in 2008-9.

2 Description of Procedure

The in-situ t_0 fitter described earlier fits simultaneously for hit time offsets and segment parameters for segments passing through single chambers. We have taken this code and created a standalone ROOT-based port of it. In addition, we have created a simple simulation of the geometry of a single chamber. Specifically, we have implemented a typical MDT big wheel chamber, with six layers in two multilayers, and tubes in sixteen mezzanine cards. With this setup, we can generate and fit straight line segments. This allows us to examine the effect of our package in correcting for various infelicities mentioned earlier, such as the jitter. In addition, we may find effects of various calibration effects upon segment performance. Schematically, our procedure is detailed in Fig. 3:

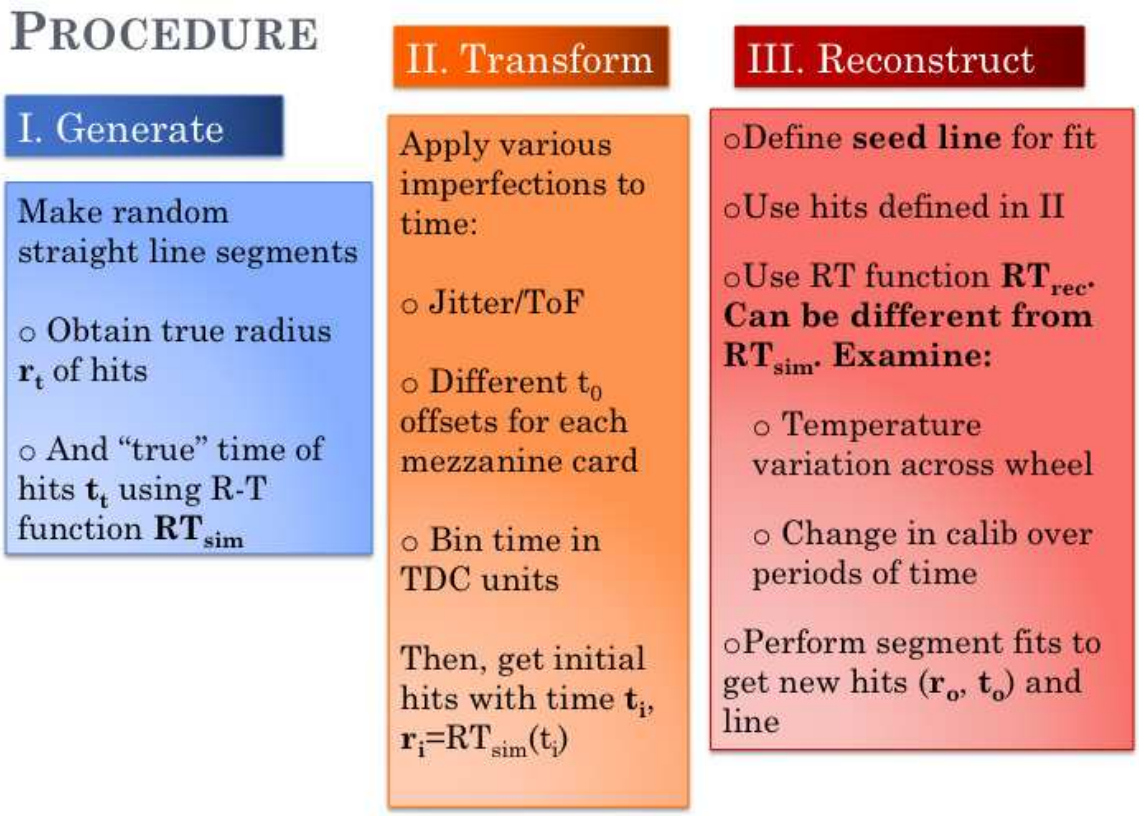

Figure 3: Procedure schematic

In detail. We begin by generating straight line segments in point-slope form, by generating the point as a flat distribution in *x*-*y*, and the angle as a flat distribution in $[0, \pi]$. From the intersection of the line segment with the drift tubes in the chamber, we get a set of hit radii $\{r_t\}$. We do *not* directly simulate hit times; instead, we use an RT^{-1} function, $\mathrm{RT}^{-1}_{\mathrm{sim}}$ to generate the "true" hit time from the radius. This gives us the corresponding set of hit times, $\{t_t\}$.

To understand the effect of various factors that can degrade the performance, we apply imperfections to the above *times*. For example, we add a jitter or time of flight effect to all the hits. Similarly, we add mezzanine card level time offsets to the hits to simulate the effect of having only chamber level calibrations. Such transformations give us times $\{t_i\}$ and radii $\{r_i = \mathrm{RT}_{\mathrm{sim}}(t_i)\}$.

We also define a seed line for the fit, which may differ from the true line in position or angle. This gives us a probe into the robustness of the segment fitting procedure assuming imperfections of pattern finding. We can account for imperfections in the *time-to-radius* conversion by using a different RT function, $\mathrm{RT}_{\mathrm{rec}}^{-1}$ to scale the hits during the fit. Finally, we fit to the transformed hits, using the seed line defined and the reconstruction RT function, and obtain fitted hits $\{r_o\}$ / times $\{t_o\}$, and segment angle and position. These may be compared to the true values to understand the extent to which the various effects above lead to a degradation in segment performance. An example segment fit is shown in Fig. 4.

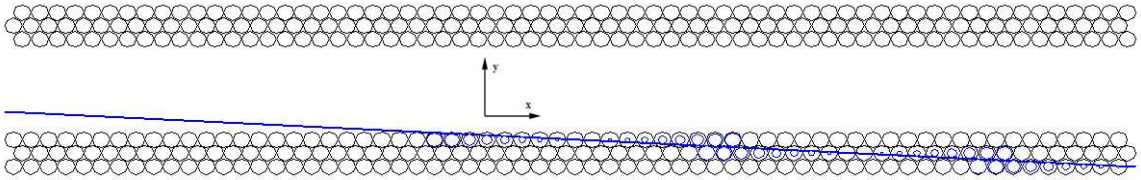

Figure 4: Display of a segment fit

3 Performance

3.1 Timing performance

We would like first to get a handle on the best-case performance of the segment fitting code in the case where there is no deformation imposed upon the hits, the seed segment is perfect, and where the same RT function is used to both make and reconstruct hits. Clearly, this is the best possible performance given the code and fitting routine. In Fig. 5 we see that in this case the residual of the segment hits is at the sub-micron level, at 0.6 μm. In addition, 97% of the hits are in this peak region.

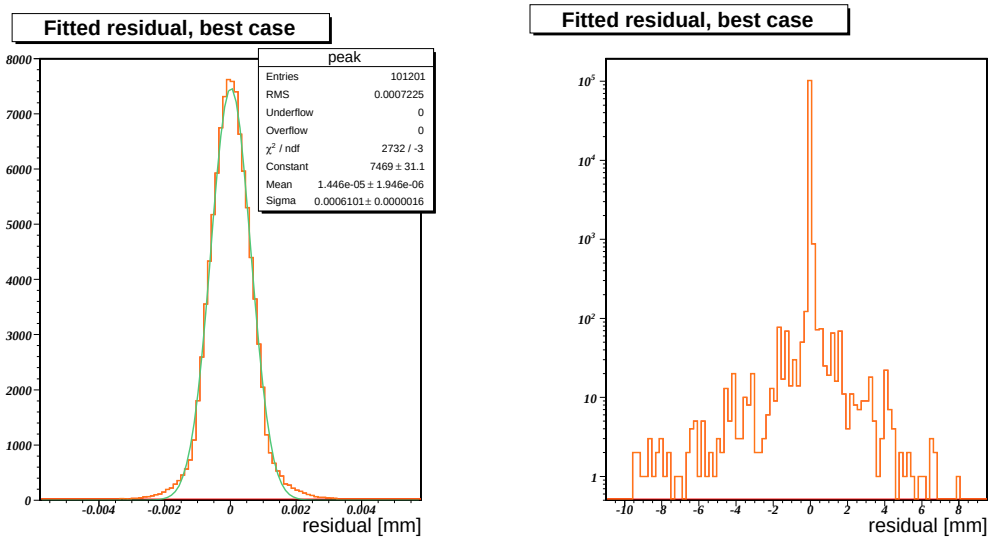

(a) Peak.

(b) Tail.

Figure 5: Performance of the code in the ideal case. We see the peak on the left, and the tails in log mode on the right

3.2 Jitter

More interesting is the situation the algorithm is designed to correct, that of timing jitter. To simulate this, we modify the true times randomly with a flat 25 ns distribution:

$$t_i = t_t + \text{rand}(-12.5, 12.5) \text{ ns} \tag{1}$$

Note that all the hits on the segment are modified by the same jitter, so that we expect to be able to correct for this effect in our fit. Indeed, as Fig. 6 shows, our hit residual is undegraded, at 0.6 μm, for a region corresponding to 94% of the hits. This is good evidence that the code functions in a satisfactory manner in correcting for jitter.

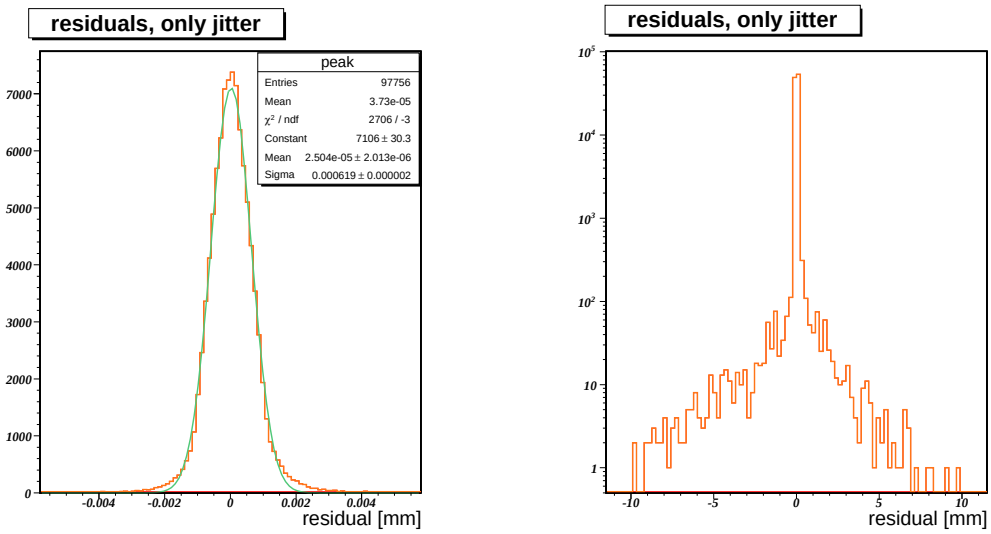

(a) Peak.

(b) Tail.

Figure 6: Performance of the code, with jitter simulation. The peak has a width of 0.6 μm as in the ideal case.

More explicitly, we find that the difference between the generated jitter and fitted t_0 shift is negligible, as seen in Fig. 7.

To get a handle on the smallness of the residuals seen with just jitter, we remind ourselves that the TDC chips on the mezzanine card bin the output times in units of the TDC fine time, 0.78125 ns. Mathematically, to simulate this effect, we set:

$$t_i = t_t + \text{round}(t_t/0.78125) \times 0.78125 \text{ ns} \tag{2}$$

This is a small effect, of course, but note that since it's a random round-off to each hit, it is an effect the segment finding could not in principle correct for. Indeed, as Fig. 8 shows, the residual width of 5.8 μm is much larger than that seen with just jitter. We note parenthetically that this number itself is plausible: for a flat rounding-off to the TDC fine count, and using 20 μm/ns as an approximate RT function, $0.78125\text{ns}/\sqrt{12} \times 20\ \mu\text{m/ns} = 4.5\ \mu$m, in good accord with the observed value. Thus reassured about the timing-related performance of our procedure.

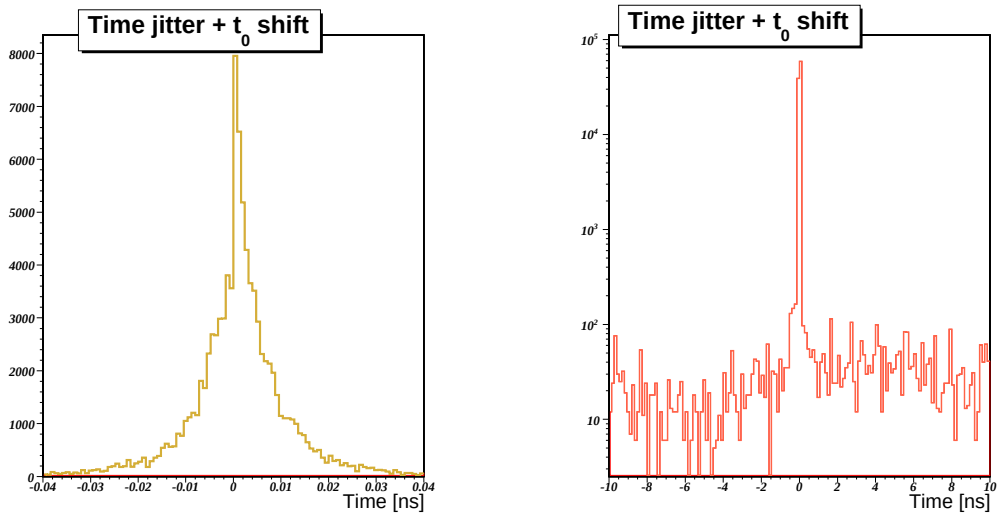

(a) Peak. (b) Tail.

Figure 7: Performance of the code, with jitter simulation. For 93% of hits, the fitted t_0 shift is within 50 ps of the generated jitter.

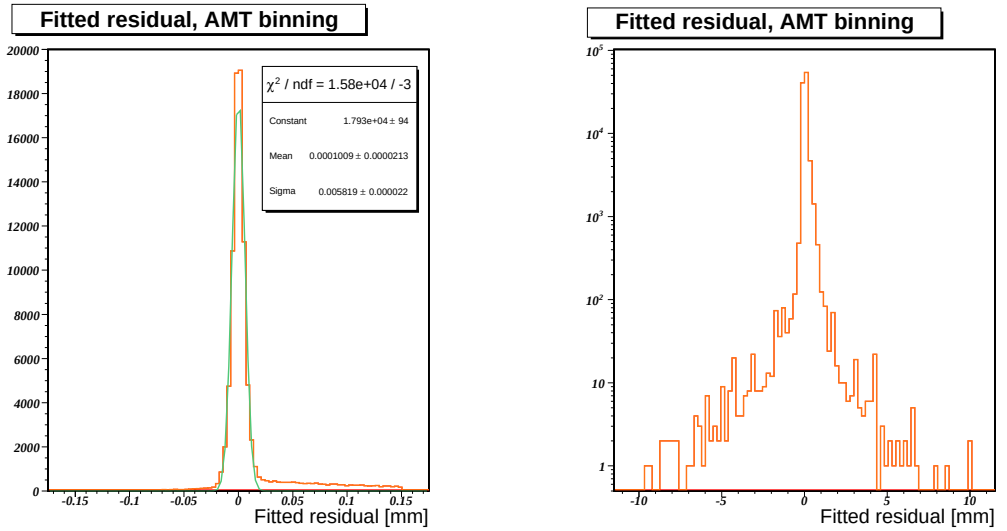

(a) Peak. (b) Tail.

Figure 8: Performance of the code, with simulation of TDC count discretization. The peak has a width of 5.8 μm, an effect an order of magnitude larger than that seen with just jitter.

3.3 Spatial performance

We also exhibit the performance of the code under deformation of the seed segment, by morphing it by ± 5 deg. In other words, we take the true segment, and rotate it about its midpoint to generate the fitting seed, as shown in Fig. 9. Mathematically, we have:

$$\theta_i = \theta_t + \text{rand}(-5,5)^\circ \tag{3}$$

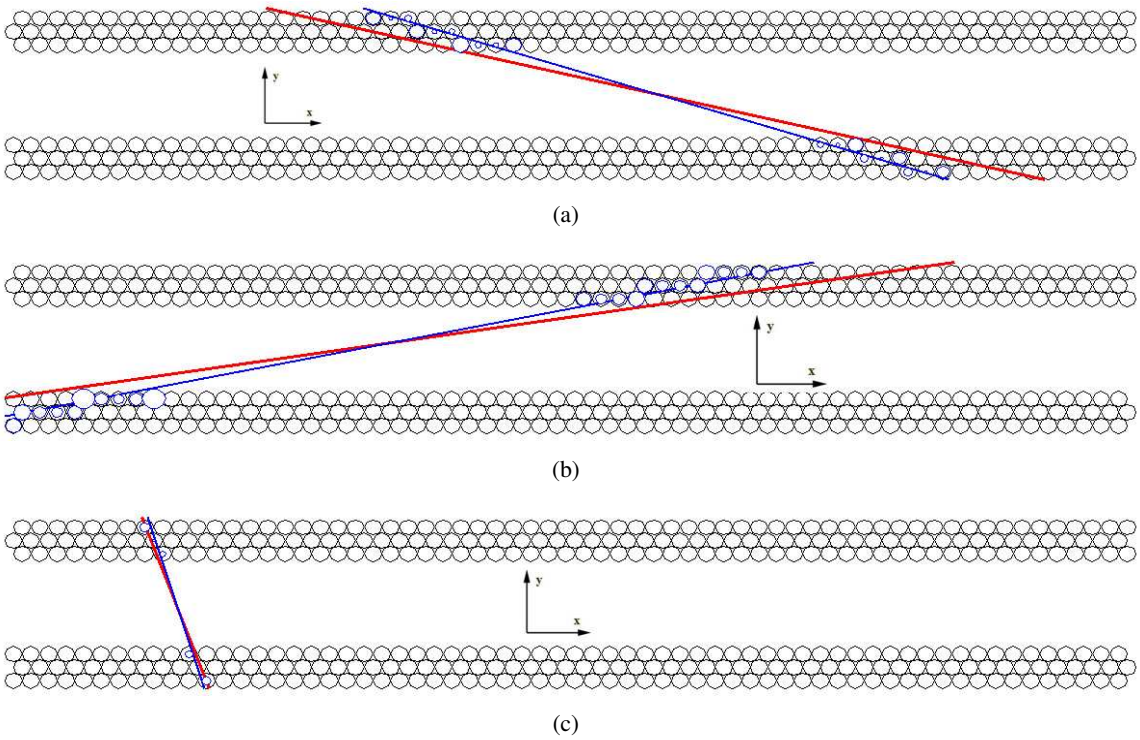

Figure 9: Morph seed segments by rotating. The red (thick) lines are the seed segments passed to the fit, while the blue (thin) lines are the returned segments

The resulting residual is shown in Fig. 10, and shows no degradation in the peak. The portion of the hits with residual larger than ± 5 μm rises to 16%.

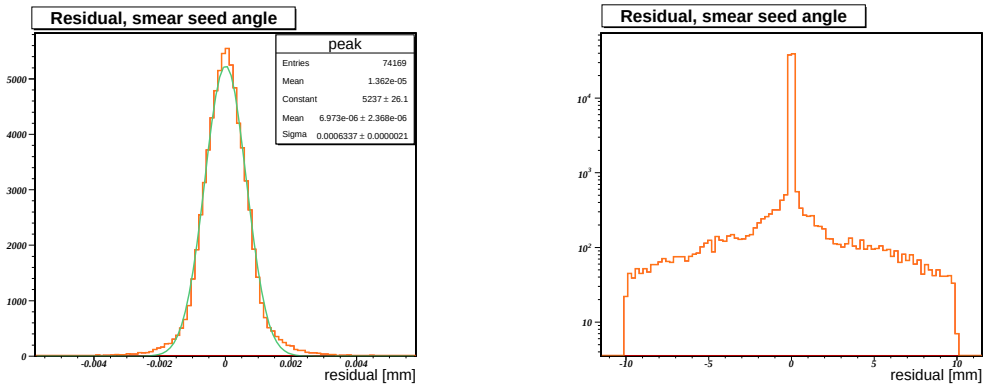

(a) Peak. (b) Tail.

Figure 10: Performance with smearing of seed angle. The peak remains undegraded.

The performance in the angle is shown in Fig. 11, where we see that the difference in angle between the true and reconstructed segment has a width of 1.05×10^{-6} rad $= 0^{\circ} : 0^{'} : 0.022^{''}$. Note however that these results correspond to flat smearing of angle, and that a more realistic result can be seen from using the different tangent lines to the drift circles, as done in the athena code.

Another important check is of the reliability relative to *position* of seed segment. We simulate this by randomly moving the seed position of the segment by ± 3 cm in x and y separately. A display is shown

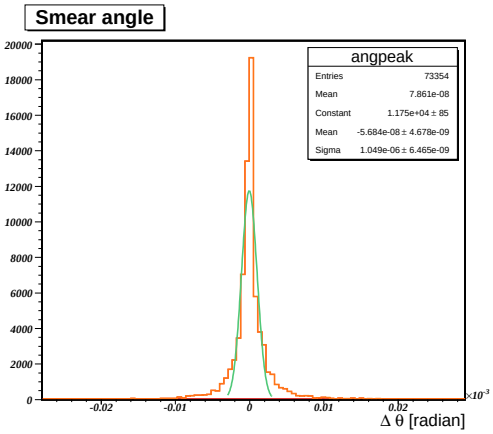

Figure 11: Difference between reconstructed and true segment angle, with smearing of seed segment.

in Fig. 12. Mathematically:

$$x_i = x_t + \text{rand}(-30, 30) \text{ mm} \tag{4}$$

$$y_i = y_t + \text{rand}(-30, 30) \text{ mm} \tag{5}$$

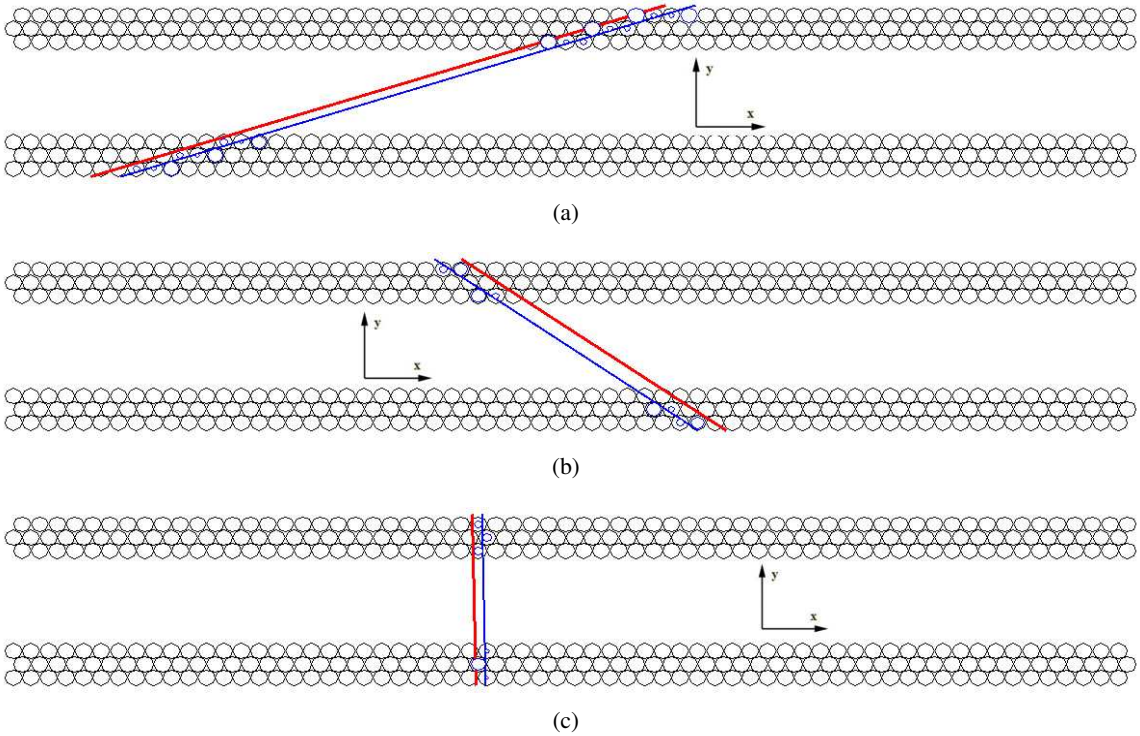

Figure 12: Morph seed segments by rotating. The red (thick) lines are the seed segments passed to the fit, while the blue (thin) lines are the returned segments

In this case, we again find that the central peak is not degraded from the optimal case, and that 91% of the hits are found with residual less than ± 5 μm, as can be seen in Fig. 13.

Note that this case corresponds to a parallel seed segment, where conceivably actual shifts in segment

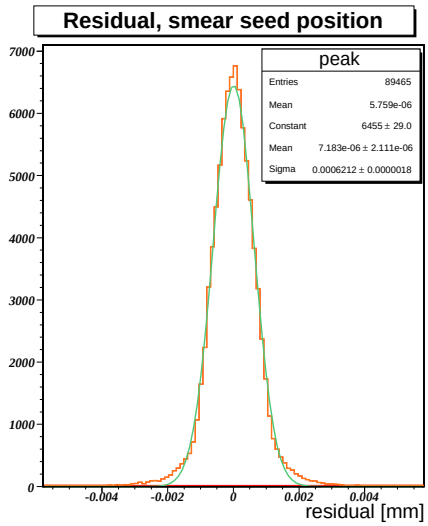

(a) Peak.

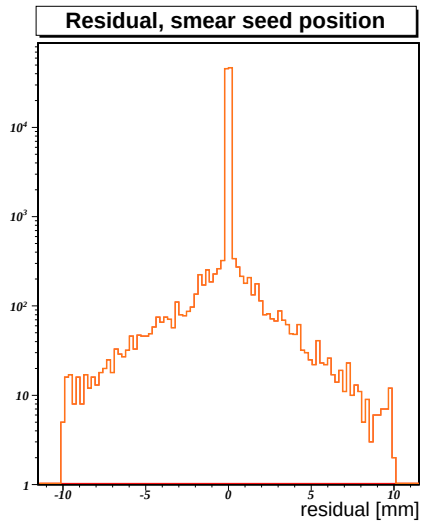

(b) Tail.

Figure 13: Performance with smearing of seed position. The peak remains undegraded.

position might be corrected for by shrinking or expanding the hits, which is to say by generating an artificial, unphysical t_0. To satisfy ourselves that this is not so, we exhibit distributions of the fitted t_0 shift in Fig. 14:

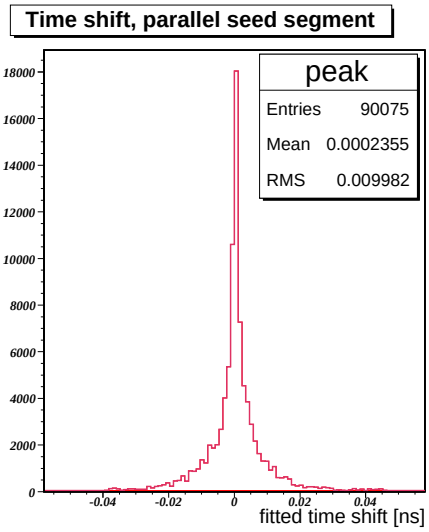

(a) Peak.

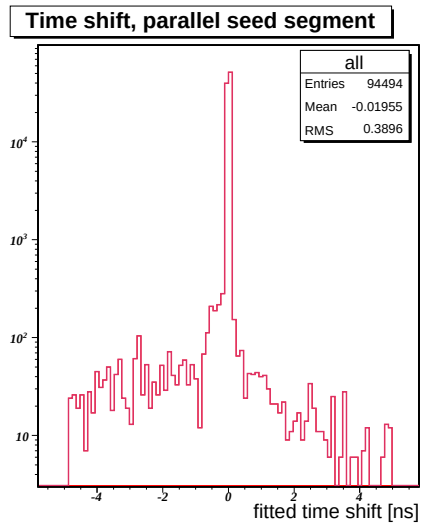

(b) Tail.

Figure 14: t_0 shift with smearing of seed position. Behold the peak at zero.

Finally, we observe that the tails in Fig. 13(b) for deformation of seed position are smaller than those in Fig. **??** for rotation of segment seed. To understand this better, consider that deformation of seed position affects all the hits on segment comparably, while rotation disproportionately affects hits far away from the point of rotation. This is graphically seen in Fig. 15.

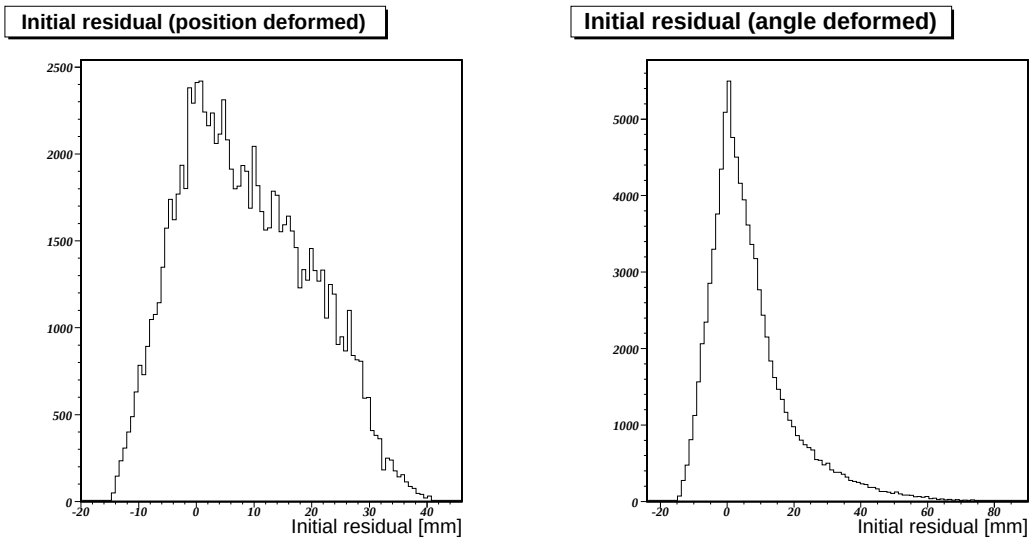

(a) Position deformation

(b) Angle deformation

Figure 15: Hit residual against seed segment, before t_0 fitting. Observe the larger tails in the angle deformation case.

3.4 Fine-graining of t_0 information in the database

It is expected and dearly to be hoped that at time of data-taking we shall have t_0 timing information at tube or at least mezzanine card scales. This is important because the cables running from the mezzanine cards to the CSM have different lengths for the different mezzanine cards, leading to different delays. This is graphically shown in Fig. 16, where we plot measured t_0 information at the mezzanine card scale for two sectors of the EM C-side wheel, from milestone week runs taken in mid-2007. We can observe $O(10\text{ ns})$ t_0 differences within a chamber.

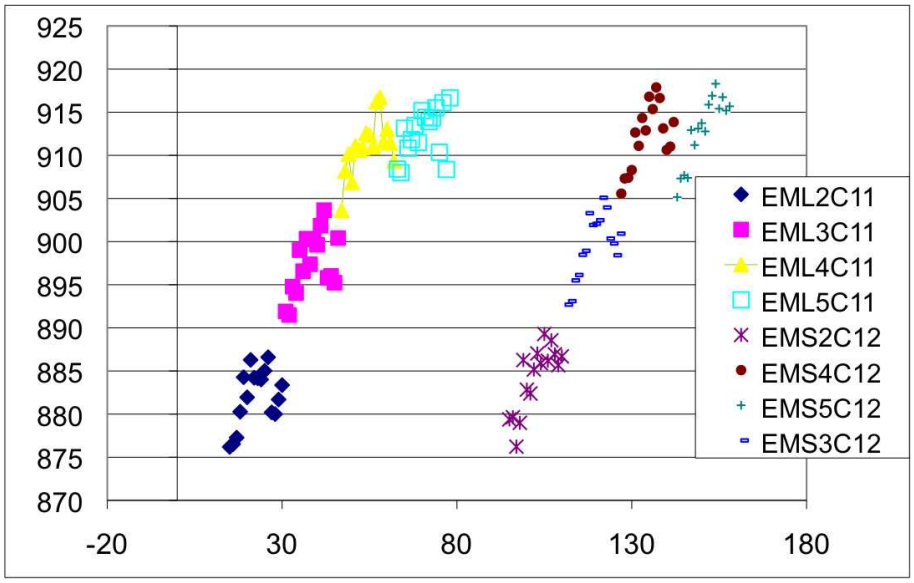

Figure 16: t_0 variation within a chamber

To emphasize the importance of providing t_0 information at this detail, we implement the case where they are *not* provided. That is, we now modify the times for the segment hits by an offset that depends on the mezzanine card that the hit corresponds to. The specific offsets have been taken from the data shown in Fig. 16, for chamber EMS5C12. As we can see in Fig. 17, the effects of this uncorrected deformation are large; we see both a width of about 30 μm and moderate tails.

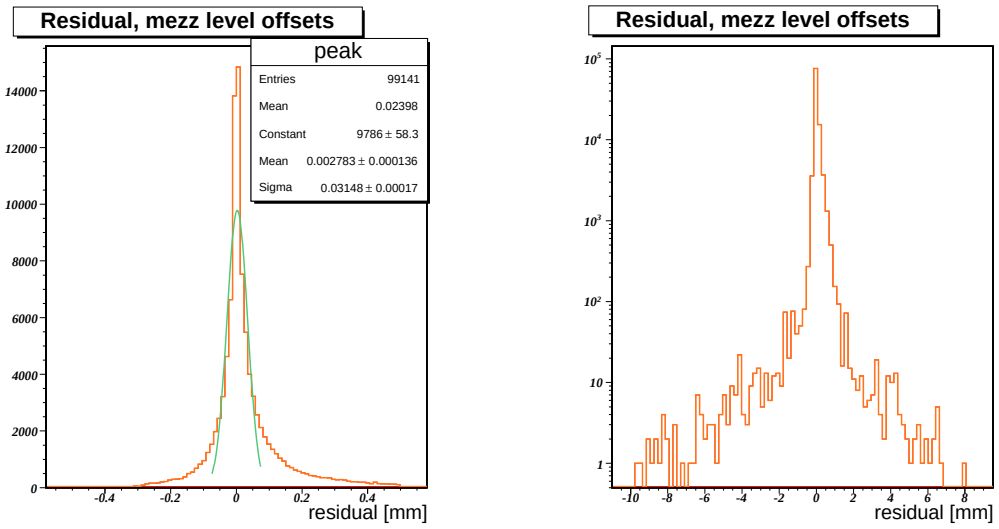

(a) Peak. (b) Tail.

Figure 17: Simulation of uncorrected mezzanine-card level t_0 differences. The peak is broad, width 30 μm, with broad tails.

However, we recall that such an effect naturally grows larger depending on the number of mezzanine cards traversed by the segment! It is instructive therefore to subdivide the data depending on this, as in Fig. 20 and Fig. 21. First, as we may see in Fig. 20(a), the case where a segment traverses only one mezzanine card shows *no* degradation in performance, as we might expect, given that a single mezz-card level offset is equivalent to jitter for our purposes. Observe that as we might expect, the width of the distribution rises in the fits as the number of mezzanine cards rises. For a typical segment, we should expect to see one, two, three or four mezzanine cards hit, though other numbers are also possible.

In Fig. 18 and Fig. 19 we see the number of mezzanine cards on barrel and endcap segments for cosmic ray data taken in run 91060, reconstructed using release `14.5.2`. For these cosmic data, we see that segments have predominantly 1-4 mezzanine cards.

3.5 Effect of out-of-date RT function

As mentioned earlier, we expect RT functions to be given for the chambers at regular intervals. To understand the effect of having out of date RT calibration, we present the effect of simulating hits with an RT function, but reconstructing with another that is for a different period. Specifically, we consider all RT functions produced at the University of Michigan Calibration Center, in 2009 through 8th May. We take all pairs of RT functions separated by a unit of time Δt, use the first function as RT $_{\text{sim}}$ to simulate segments and hits, and the next one as RT $_{\text{rec}}$ to fit the segment and hits.

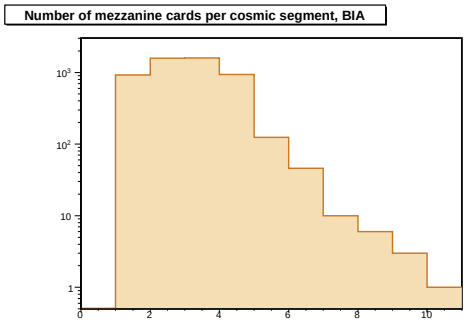

(a) BI chambers, A-side.

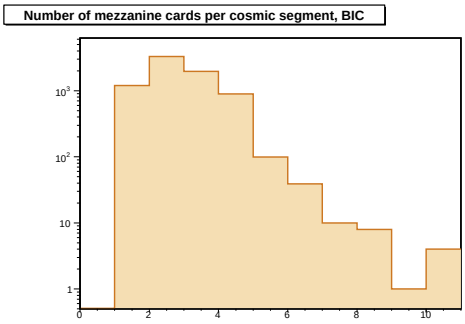

(b) BI chambers, C-side.

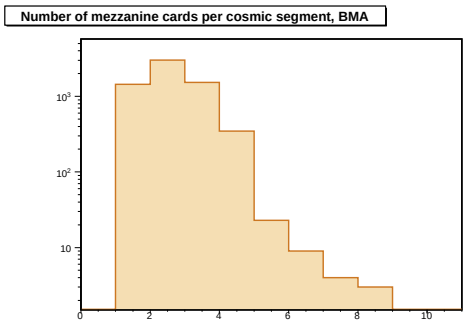

(c) BM chambers, A-side.

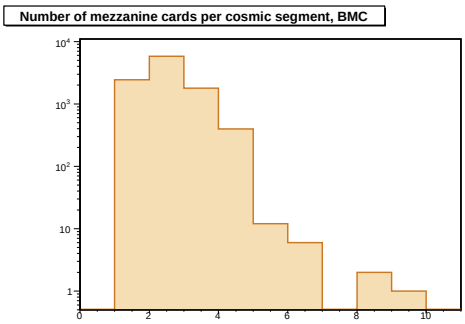

(d) BM chambers, C-side.

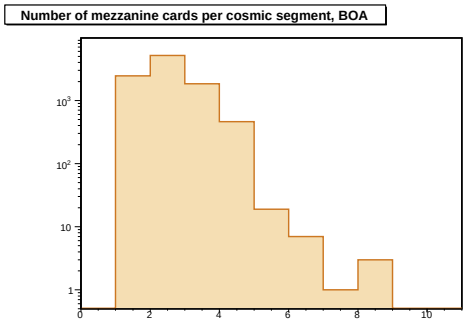

(e) BO chambers, A-side.

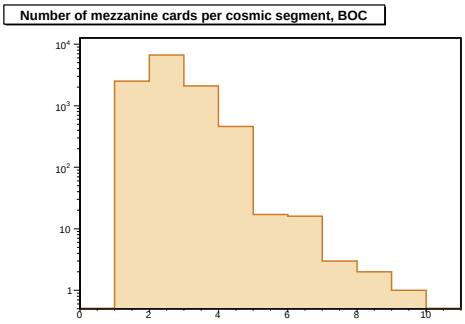

(f) BO chambers, C-side.

Figure 18: Number of mezzanine cards per barrel segment, cosmic data run 91060

First, we consider a 12 ± 0.5 hour difference in RT calibration functions. For the 252 pairs of such RT functions in our time period, we exhibit the mean and RMS values of the hit-on-segment residual distribution, in Fig. 22. We observe that being out-of-date by this time period tends to create an effect in the segment resolution up to the order of 10-20 microns.

We note that the structure in the plots, considered in the next section, comes from periods of time when the gas composition and conditions change significantly. One instance of 12-hour time difference is shown in Fig. 23, where we see a central width of 6.6 μm.

To give a starker example, we consider the case where RT functions are off by a week. Specifically, we consider pairs of functions separated in time by 7 days $\pm$ 10 minutes. For the 337 such pairs in our

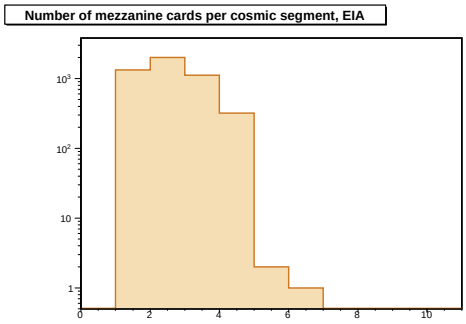

(a) EI chambers, A-side.

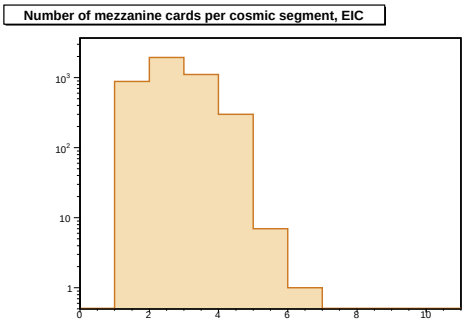

(b) EI chambers, C-side.

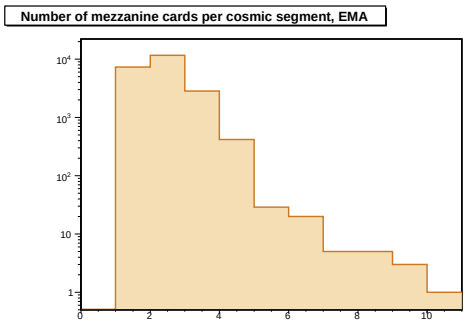

(c) EM chambers, A-side.

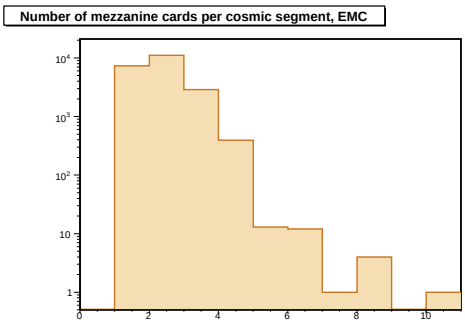

(d) EM chambers, C-side.

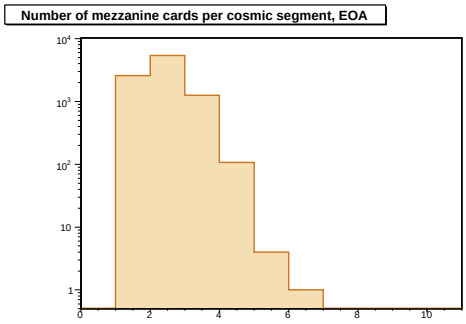

(e) EO chambers, A-side.

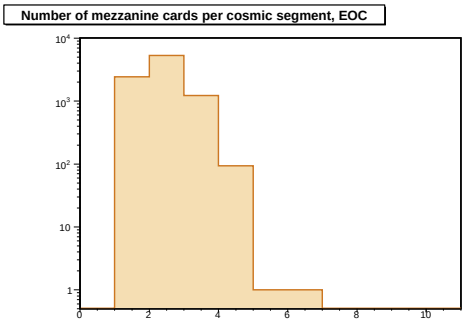

(f) EO chambers, C-side.

Figure 19: Number of mezzanine cards per endcap segment, cosmic data run 91060

sample, we again simulate segments with the first and reconstruct with the second. The results are shown in Fig. 24, where we see that the effect of unchecked gas conditions over such a time period can be on the order of 50 - 100 microns.

A particular case is seen in Fig. 25, where we see an RMS value of 54 μm. Note that the distribution of residuals is highly non-gaussian.

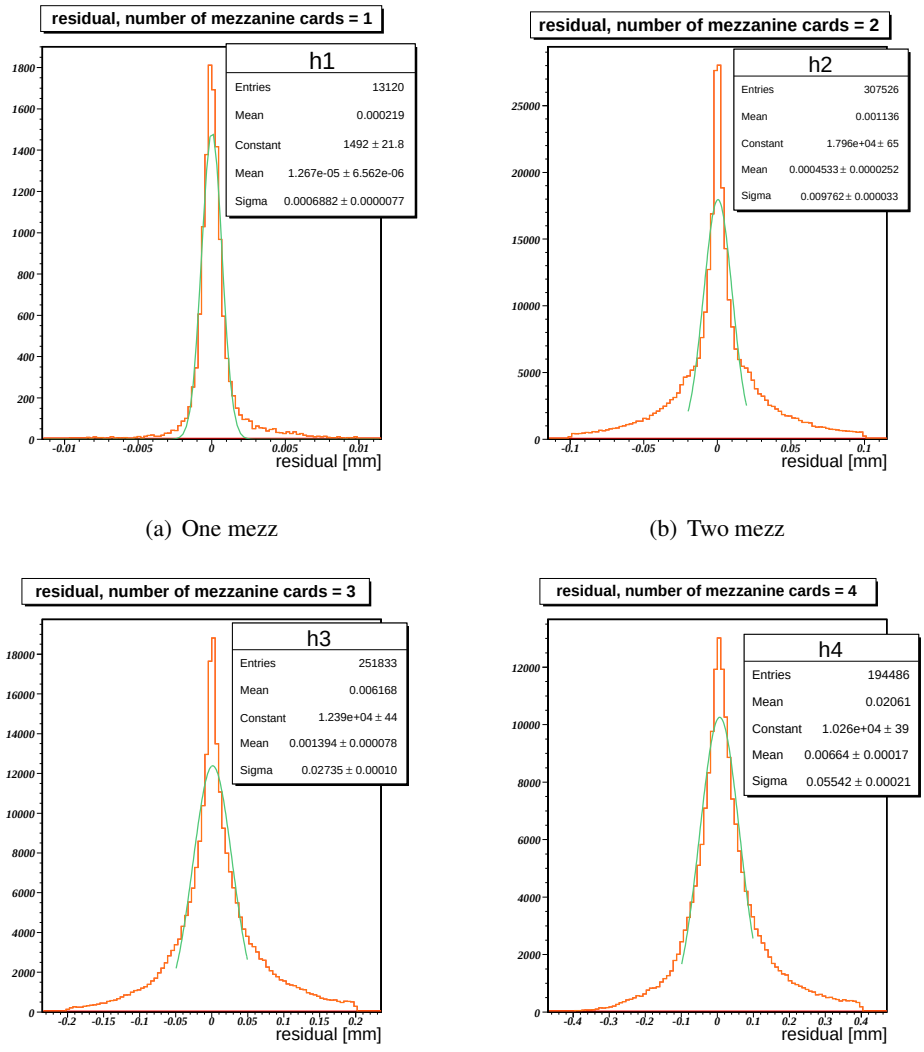

(a) One mezz

(b) Two mezz

(c) Three mezz

(d) Four mezz

Figure 20: Simulation of uncorrected mezzanine-card level t_0 differences. Residuals depending on number of mezz cards traversed by the segment

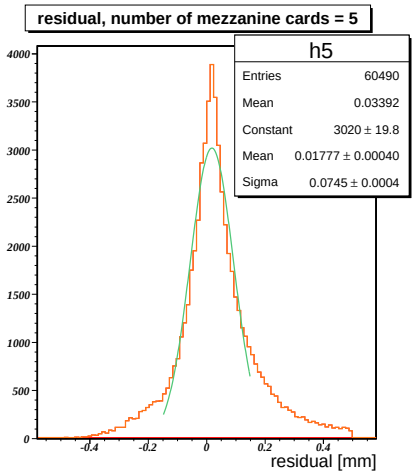

(a) Five mezz

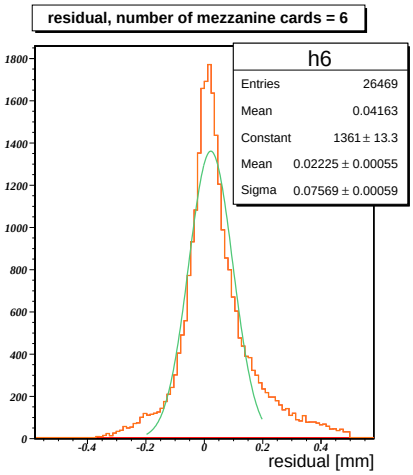

(b) Six mezz

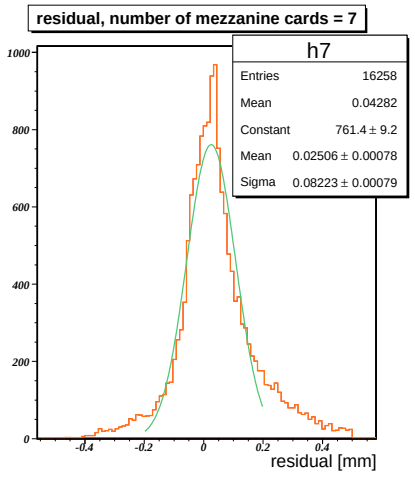

(c) Seven mezz

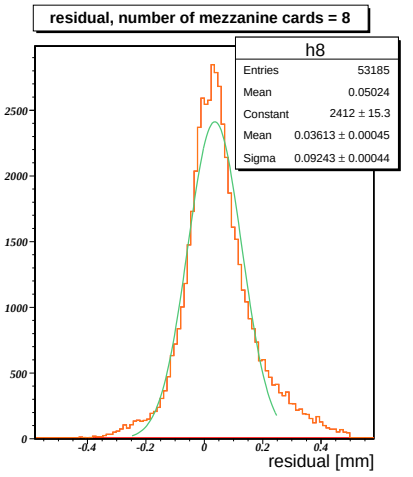

(d) Eight mezz

Figure 21: Simulation of uncorrected mezzanine-card level t_0 differences. Residuals depending on number of mezz cards traversed by the segment

Number of Mezzanines	Central Width	Percent of Cosmic Segments
1	0.7 μm	27%
2	9.8 μm	52%
3	27.4 μm	17%
4	55.4 μm	3.5%
5	74.5 μm	0.22%
6	75.7 μm	0.009%
7	76.1 μm	0.002%
8	92.4 μm	0.002%

Table 1: Segment residual versus number of mezzanine cards traversed.

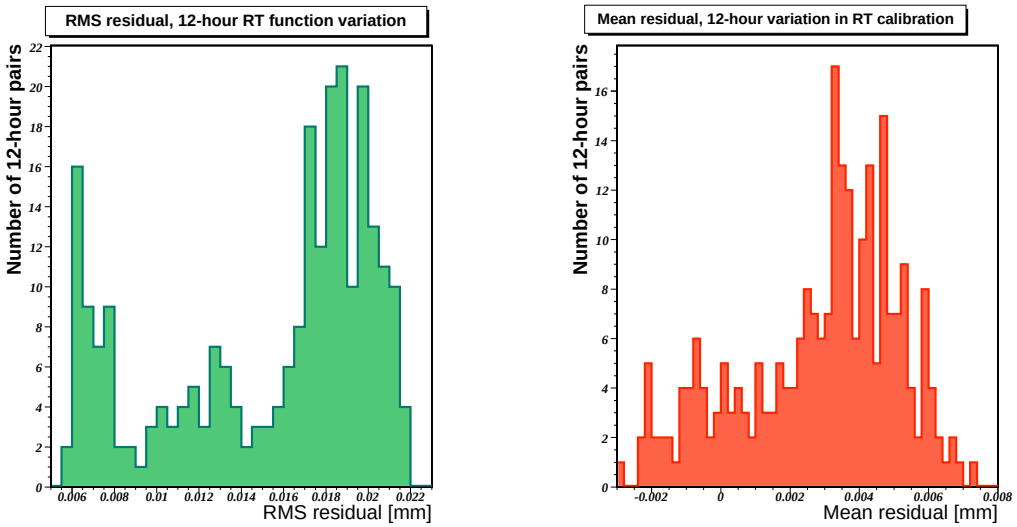

(a) RMS.

(b) Mean.

Figure 22: Simulation of RT functions out-of-date by 12 hours. Each data point on these plots corresponds to one pair of RT functions differing in time by 12 hours, for which an iteration of our simulation/fit procedure is performed. The left plot shows the RMS of the residual distributions seen for all the different iterations. On the right we see the mean of these residual distributions.

3.6 Monitoring RT function changes and effect on residuals via TDC spectra

As we have just seen, the effect of gas conditions upon segment residuals is profound, in that even a 12-hour difference from the *true* RT function can impose a 10-20 micron effect upon the segment residuals. Note that this is an effect in addition to the the question of the extent to which gas conditions are accurately modeled by well-calibrated RT functions: stipulating that a good RT function models the gas conditions in a tube perfectly, we still see the effects of the previous section.

Hence, it is desirable to have a probe upon such effects, which we seek in terms of TDC spectra. The modus operandi is to consider cases where we identify large impact upon segment residuals, and for such cases, try to correlate to features of TDC spectra such as the maximum drift time, the slope of the rising and falling edges of the distribution etc.

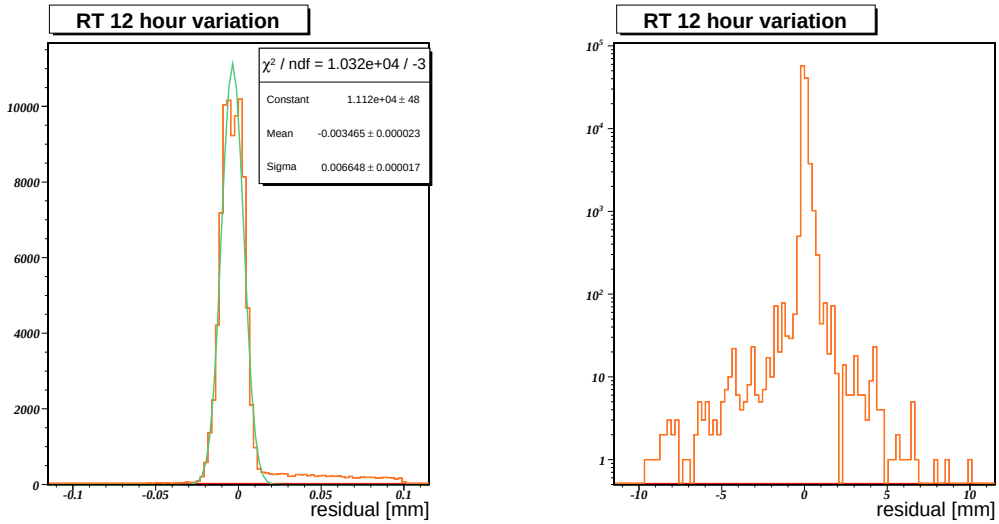

(a) Peak. (b) Tail.

Figure 23: Performance of the code, with 12-hour old RT calibration. The peak has a width of 6.6 μm.

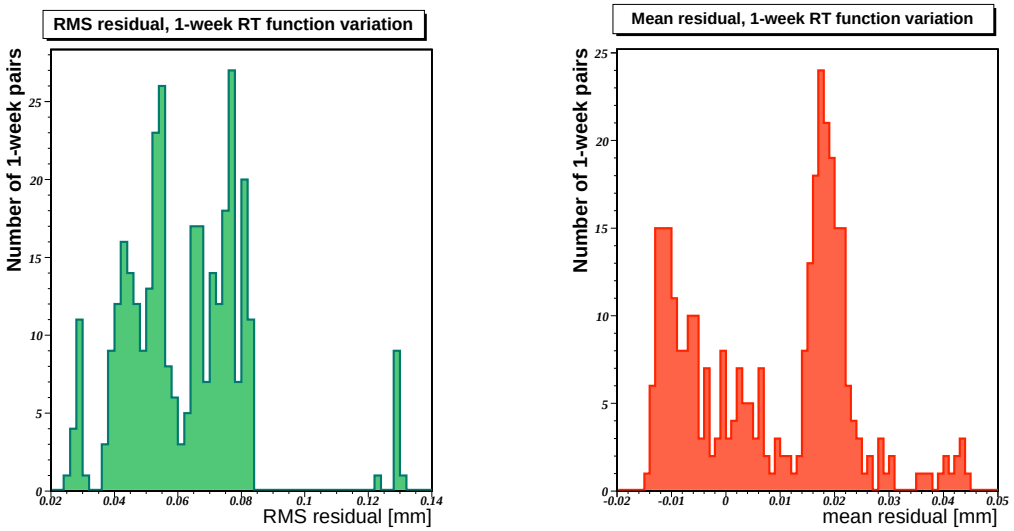

(a) RMS. (b) Mean.

Figure 24: Simulation of RT functions out-of-date by one week. Each data point on these plots corresponds to one pair of RT functions differing in time by a week, for which an iteration of our simulation/fit procedure is performed. The left plot shows the RMS of the residual distributions seen for all the different iterations. On the right we see the mean of these residual distributions.

3.7 Effect of temperature variation

We know that chamber gas temperatures may vary by O(5K) between the top and the bottom of the ATLAS detector. Naturally, these changes affect the RT functions for the reconstruction, which must be corrected for such effects. We examine here the impact upon performance of *not* using such tem-

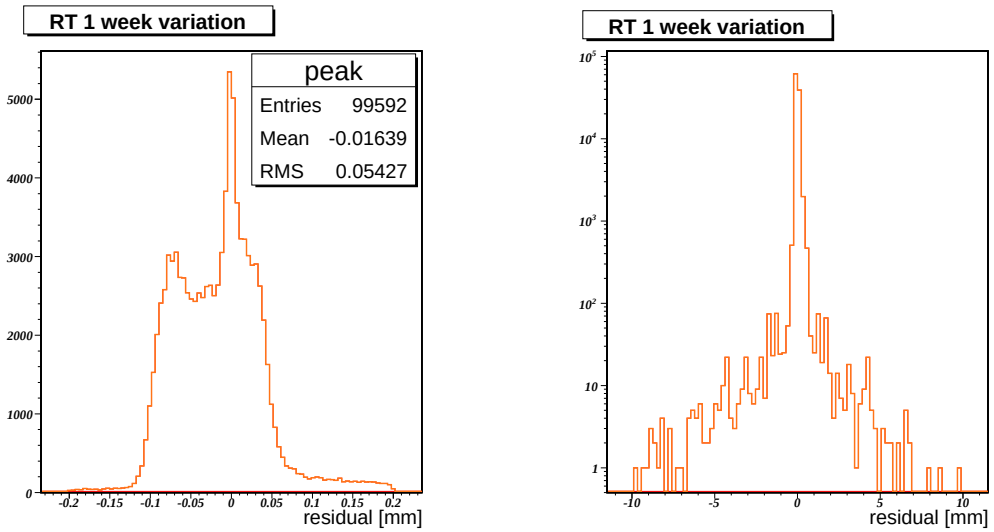

(a) Peak. (b) Tail.

Figure 25: Performance of the code, with week old RT calibration. The peak is highly non-gaussian, and has an RMS of 54 μm.

perature corrections. We get a handle on this by taking the most and least compressed temperature corrected RT functions seen across big-wheel A, and using them to simulate and reconstruct hits. The two RT functions are shown in Fig. 26.

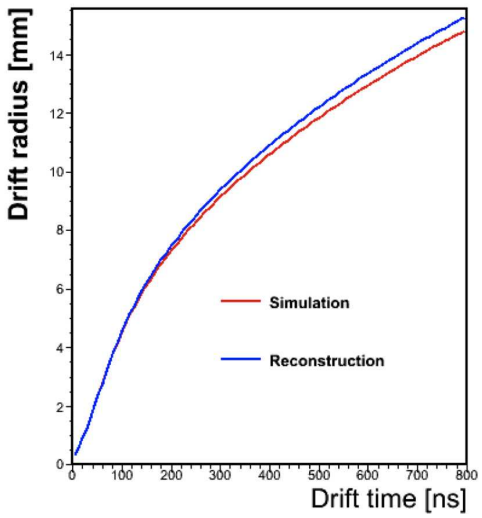

Figure 26: Simulation and reconstruction RT functions, corresponding respectively to the most compressed / coldest and least compressed / hottest chambers on endcap big wheel-A.

Observe that since our reconstruction RT function is systematically less compressed than the simulation one, the segment finding procedure thinks all hits larger than they truly are. This should skew the residuals (defined as track - hit) systematically negative. Indeed, as we observe in Fig. 27, the residuals are

in fact systematically made negative, an effect that grows larger with increasing hit radius. The overall width of Fig. 27(a) is 214 μm.

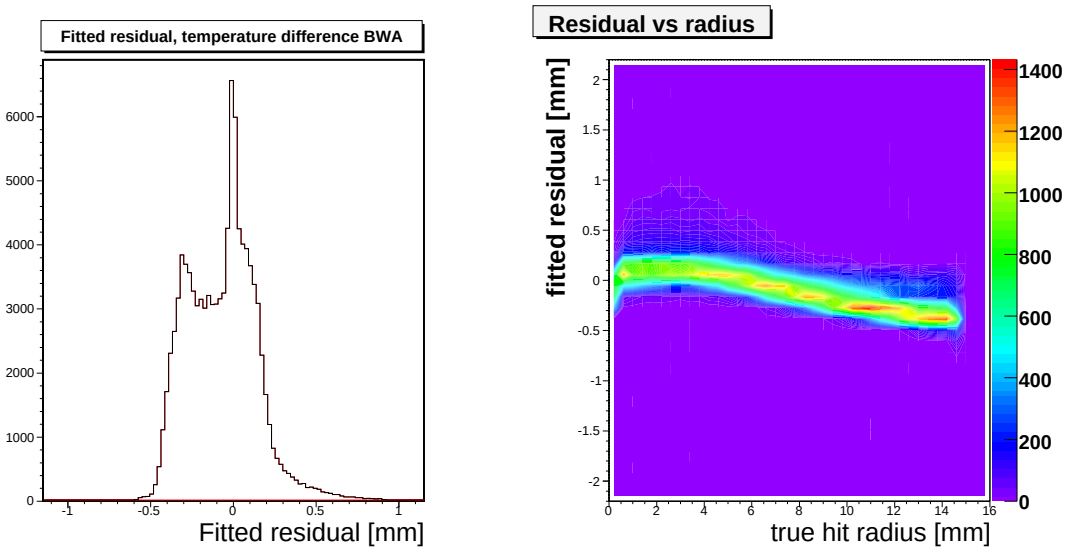

(a) residual

(b) vs radius

Figure 27: Residuals without temperature correction. Observe both the large width, and the non-gaussian shape, with RMS of 214 μm.

Given the radius dependence of the shift in mean, we separate our result for small and large radius, with a split at 9 mm. Note that in each case we see widths greater than 100 μm. Further, the large radius plot exhibits a mean shift, corresponding to the fact that the reconstruction RT function is broader than the one used to simulate.

4 Summary

It appears that the intrinsic residual width imposed by the segment fitting code is sub-micron, and that purely jitter based effects are entirely corrected for without imposing a penalty in hit residual. Further, we emphasize the vital significance of providing temperature corrected, up-to-date RT functions and desirability of mezzanine-card level t_0 calibration.

5 Acknowledgements

We gratefully acknowledge the assistance provided by Dan Levin, who provided us with temperature corrected RT functions, and gave detailed responses to several questions.

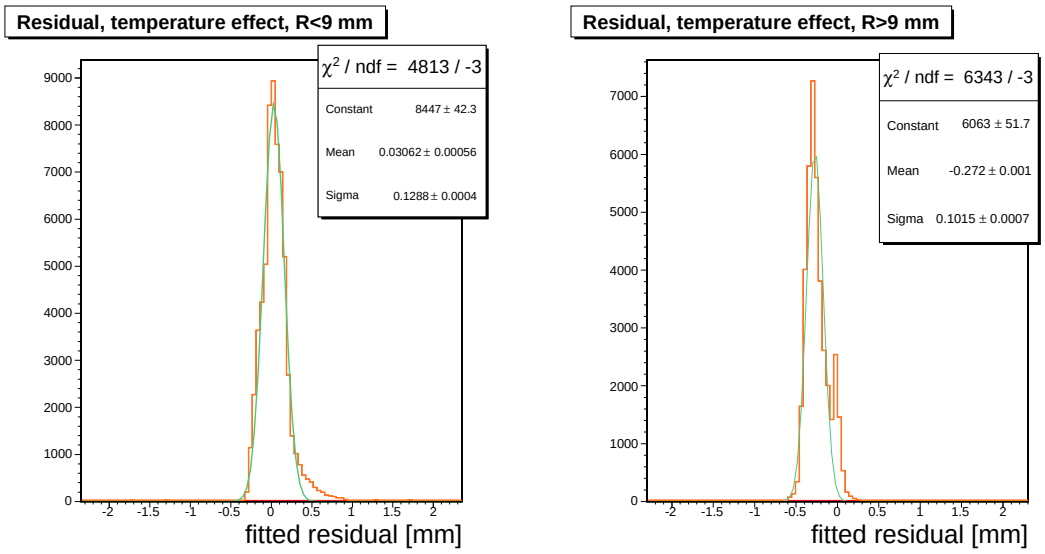

(a) residual, small radius

(b) residual, small radius

Figure 28: Residuals without temperature correction, for small and large radius. In each case, we observe widths greater than 100 μm. In addition, the large radius plot exhibits a mean shift, corresponding to the fact that the reconstruction RT function is broader than the one used to simulate.

References

[1] A. Belloni, K.M. Black, J. Guimaraes da Costa, V.I. Martinez Outschoorn, S. Prasad, In-situ t_0 calibration for MDT segments, April 2009, ATL-COM-MUON-2009-006.